Heliyon 6 (2020) e03323

Contents lists available at ScienceDirect

Heliyon

journal homepage: www.cell.com/heliyon

Research article

Green synthesis of Copper Oxide/Carbon nanocomposites using the leaf extract of *Adhatoda vasica* Nees, their characterization and antimicrobial activity

P.G. Bhavyasree [a,b,c], T.S. Xavier [b,c,*]

[a] *Department of Physics, S.N College, Chathannur, India*
[b] *Center for Advanced Materials Research, Department of Physics, Govt. College for Women, Thiruvananthapuram, Kerala, India*
[c] *University of Kerala, India*

ARTICLE INFO

Keywords:
Materials science
Green synthesis
Plant extract
Copper oxide/Carbon nano composites
Antimicrobial activity
Adhatoda vasica

ABSTRACT

Copper Oxide/Carbon (CuO/C) nanocomposites were developed through the green method using the leaf extract of *Adhatoda vasica* at room temperature. Here, the leaf extract serves as a capping agent, reducing agent and a source of carbon for the formation of nanocomposites. As we know, this is the first article on the synthesis of CuO/C nanocomposites using this leaf extract. The nanocomposites were prepared by mixing the copper sulphate pentahydrate solution with the plant extract under certain conditions. The synthesized material was characterized by XRD, UV-Visible, FTIR, FE SEM, EDS, XPS and TGA. The results revealed that the synthesized material is a composite of copper oxide and functionalized graphene-like carbon. The SEM images indicated that the CuO/C nanoflakes had an average thickness of 7–11nm. Further, the composites were examined for antifungal activity and antibacterial activity. The nanocomposites showed significant antibacterial activity against the pathogenic bacterial strains *Escherichia coli, Pseudomonas aeruginosa, Klebsiella pneumoniae* and *Staphylococcus aureus* and antifungal activity against the fungi *Aspergillus niger* and *Candida albicans.* Also, the Minimum Inhibitory Concentration (MIC) and Minimum Fungicidal/Bactericidal Concentration (MFC/MBC) of the nanocomposites were determined against the fungus *C. albicans* and the bacteria *K. pneumonia.*

1. Introduction

Recently, copper oxide nanostructures have drawn special consideration of material scientists because of their broad collection of applications such as sensors [1, 2], catalytic [3], optical [4], electrical [5], gas sensors [6, 7, 8], preparation of organic-inorganic nanostructure composites and solar energy transformation [9]. Further, they can be utilized as an antibacterial and antifungal agent [10]. In ancient Ayurveda, there are many pieces of literature describing the preparation and benefits of Tamra bhasma [11]. Tamra bhasma is nothing but the purified form of copper oxides. Also, there are many reports available describing the antibacterial activity of nanostructured carbon [12, 13, 14, 15]. Chen *et al.* published the antimicrobial activity of graphene oxide against bacterial phytopathogens and fungal conidia [16]. The composites of carbon and copper oxide could be an incorporation of properties of the two components which can lead to a new material bearing novel features. However, there are a few reports available about the biological activity of carbon enclosed with copper oxide nanocomposites. In 2017, Kiran Kumar *et al.* reported the synthesis of graphene oxide/copper oxide nanocomposites and the biological activity of the prepared composites [17]. Also, there are some reports available suggesting the antimicrobial activity of graphene oxide/metal hybrids [18, 19].

Nowadays, the green synthesis of nanomaterials became a better choice of scientists compared to the other synthesis methods. This is because the synthesis techniques involve eco-friendly and non-toxic procedures. In the green synthesis of nanomaterials, the plant has a better role compared to the microorganisms due to its availability and simplicity of the method of preparation. Also, the rate of production is quicker than in the case of microorganisms. There are many kinds of literature available about the green synthesis of nanostructures. J. Y. Song *et al.* reported the engineering approaches for the production of metal nanoparticles using plant extracts [20, 21]. H. J. Lee *et al.* reported the production of copper nanoparticles using the *Magnolia Kobus* leaf extract for the first time [22]. Many reports about the synthesis of

* Corresponding author.
E-mail address: xavierkattukulam@gmail.com (T.S. Xavier).

https://doi.org/10.1016/j.heliyon.2020.e03323
Received 22 November 2018; Received in revised form 20 March 2019; Accepted 24 January 2020

copper/copper oxide nanoparticles using different types of plant extracts are available [23, 24, 25, 26, 27, 28, 29, 30]. Also, some reports are describing the green synthesis of carbon nanostructures. In 2013, Mewada *et al.* reported the biological synthesis of carbon dots using the aqueous extract of *Trapa bispinosa* peel [31] and in 2018, Zhing *et al.* published the synthesis of fluorescent carbon dots from starch [32]. Also, Lu et al. published the synthesis of fluorescent carbon nanoparticles from pomelo peel [33]. In this report, we are presenting the green synthesis of CuO/C nanocomposites using the aqueous leaf extract of *Adhatoda vasica* Nees as reducing agent and capping agent. The plant extract also acts as the source of carbon [34]. As we know, this is the first article on the synthesis of CuO/C nanocomposites using the aqueous extract of A. *vasica* Nees.

The identification of *Adhatoda vasica* Nees/*Justicia adhatoda* is made with the available literature. It is a well-known plant drug used in Ayurveda. It is very commonly known as Malabar nut tree. The local names of the plant are Ya-Zui-Hua in China, Nongmangkha-agouba (Manipuri), Adasaramu (Telugu), Alduso (Gujarati), Adadodai (Tamil), Vasaka (Sanskrit), Atalotakam (Malayalam) and Adusoge (Kannada) in India. It is a small evergreen shrub having broad leathery leaves. The leaves have a light green colour on top and deep green beneath. The leaf becomes brownish-green colour when it is dried and it tastes bitter [35]. The aqueous extract of *A. vasica* leaves contain phytochemicals such as alkaloids, tannins, saponins and phenols [36, 37, 38, 39, 40, 41]. They also contain sugars, proteins and amino acids such as glycine.

Different types of characterization techniques have been employed to investigate the composition and structure of the prepared material. Also, the antimicrobial activities of the composites against the pathogenic bacterial strains *E. coli, P. aeruginosa, S. mutans, K. pneumonia* and *S. aureus* and the fungi *A. niger and C. albicans* were studied.

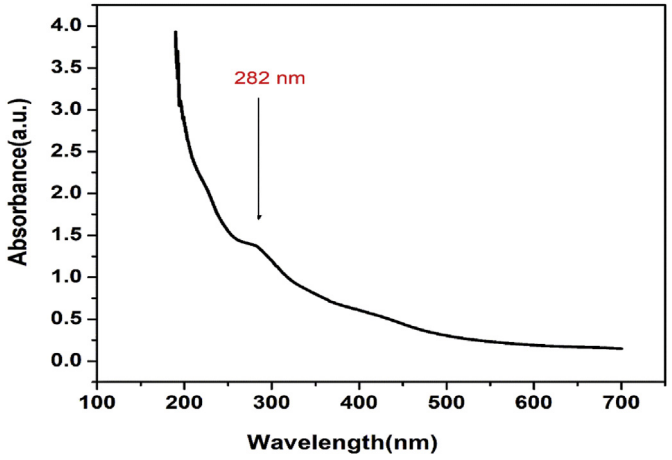

Figure 1. The UV-visible spectrum of CuO/C nanocomposites.

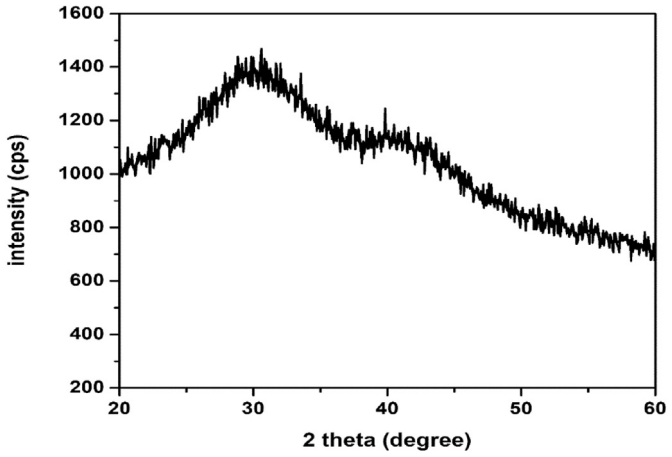

Figure 2. Powder XRD spectrum of CuO/C nanocomposites

2. Materials and methods

2.1. Plant material and preparation of leaf extract

The fresh leaves of *A. vasica* were gathered from the botanical garden of S.N College, Kollam, Kerala, India (8°52′52.07″ N and 76°35′4.88″). The leaves were properly cleaned with tap water to avoid dust and other contaminated particles and were cleaned many times by double distilled water. The leaves were shade dried for three weeks and made into a fine powder using a grinder. The crushed leaves were weighed and dispersed in double-distilled deionized water in the ratio 1g: 100 ml. The dispersion was sonicated for half an hour and then centrifuged. The supernatant solution was kept in a refrigerator and again centrifuged after 24 h. Then the solution was purified using a Whatmann No.1 filter paper to avoid all the plant residues in it.

2.2. Synthesis of CuO/C nanocomposites

Copper sulphate pentahydrate ($CuSO_4.5H_2O$) of analytical grade was purchased from Merck. The solution of copper sulphate pentahydrate was used as the source for the CuO and the leaf extract as the reducing agent, capping agent and source of carbon. In double distilled water 0.01 M copper sulphate solution was made and added to the supernatant solution of leaf extract in 5:4 volume ratio followed by constant stirring and in a nitrogen atmosphere. The experiment was repeated for different volume ratios. But the maximum yield was obtained in the ratio 5:4. So the ratio was fixed to 5:4. The reaction mixture was continued to be stirred for half an hour. Then a cloudy cluster of particles was formed. The formation of nanostructures was observed with a notable colour change [22]. The pH of the precursor solution, plant extract and the mixture solution were noted during the experiment. Then the nanocomposite solution was incubated for 24 h to complete the reaction and the residue obtained was cleaned five times with deionized water and centrifuged. The purified particles were air-dried and used for further study.

2.3. Characterization

The composition and structure of the synthesized material were analysed by UV-Visible (Shimadzu UV-1800 Spectrophotometer), XRD ("X" Pert PROPAN Analytical, model: PE3040/60), FE-SEM (JEOL-JSM 5600), EDS (FEI-Nova Nano SEM 450), XPS (Kratos Analyticals, U.K; model: Axis Ultra with Aluminium Kα), FTIR (Shimadzu FTIR Spectrophotometer, model: IR Prestige-21) and TGA (TGA-50 Detector).

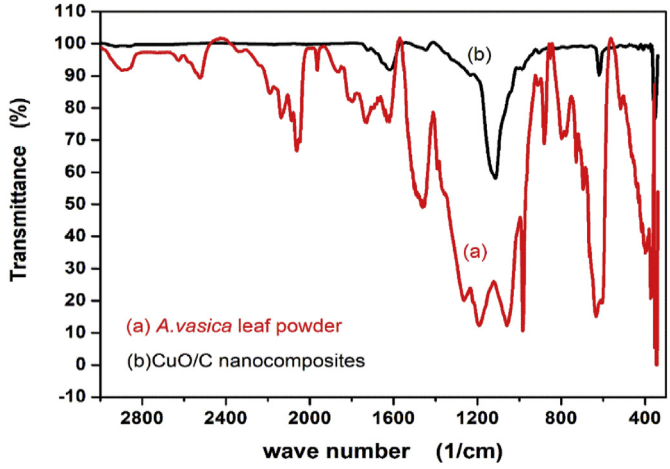

Figure 3. FTIR spectrum of *Adhatoda vasica* leaves and CuO/C nanocomposites

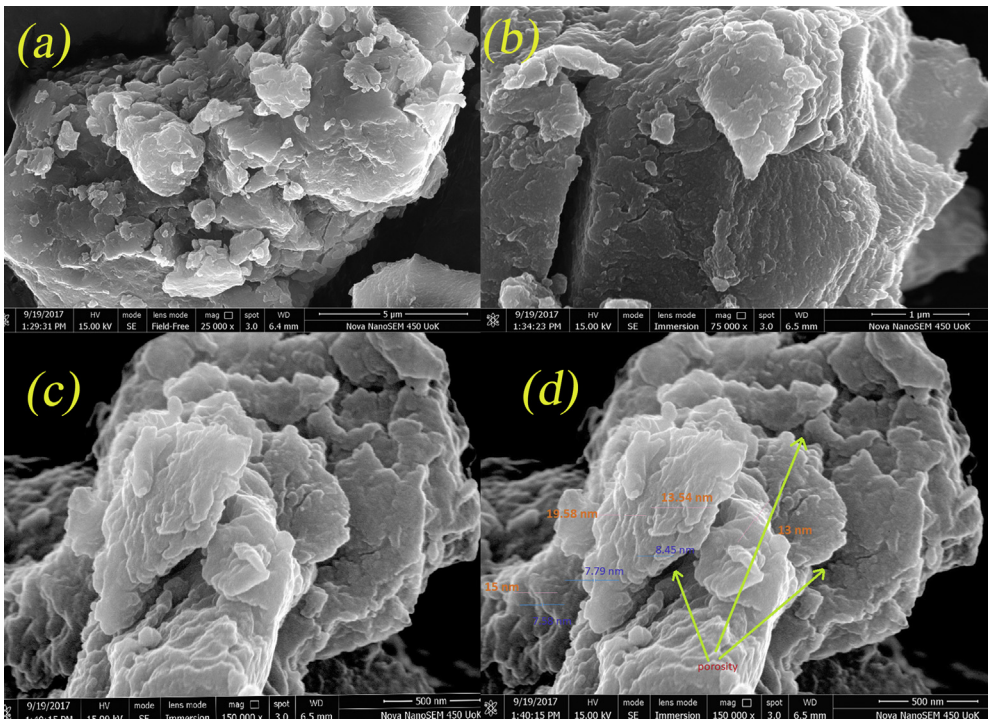

Figure 4. SEM images of CuO/C nanocomposites obtained (a) under magnification of 25000 (b) under magnification of 50000 (c) under magnification of 150000 (d) under magnification of 150000 and labelled with porosity and flake thickness.

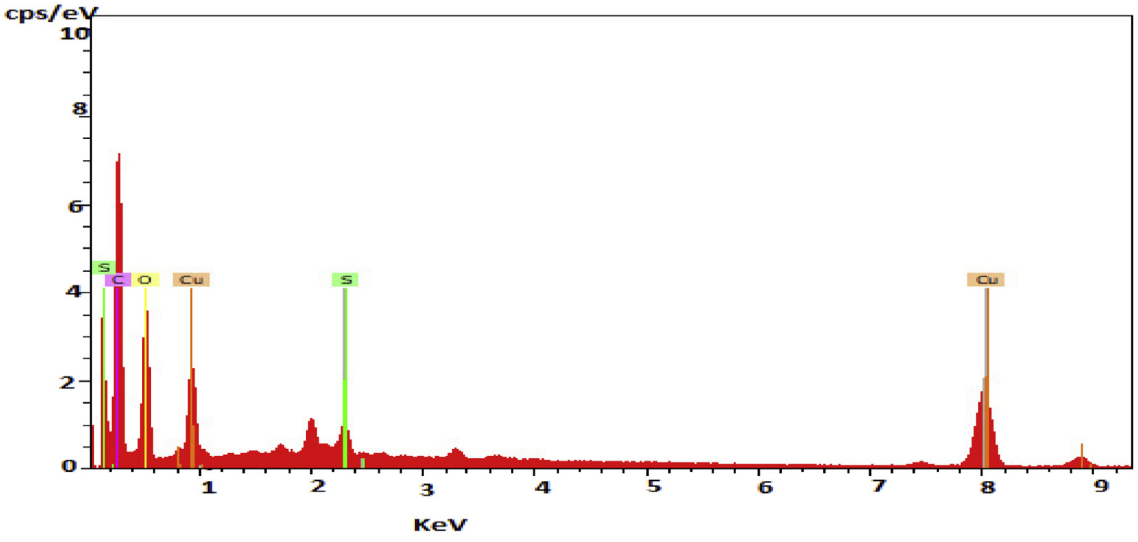

Figure 5. EDS profile of CuO/C nanocomposites

2.4. Antimicrobial test

The antimicrobial tests were conducted according to NCCLS, 1993 (National Committee for Clinical Laboratory Standards. (1993a). Performance standards for Antimicrobial Disk Susceptibility Tests-Fifth Edition: Approved Standard M2-A5. NCCLS, Villanova, PA.). The antimicrobial activity was determined by agar well diffusion method. The principle of this method is that the antimicrobials existing in the sample are permitted to spread out into the medium and these antimicrobials interact in the plate sowed with the test organisms. The resultant zones of inhibition against the organisms will be fairly circular since there will be a convergent lawn of growth. The diameter of the resulting zone of inhibition in this method can be measured in millimetres. Muller Hinton Agar Medium (MHI Agar Media) was used for bacterial culture. The medium for the antibacterial test was prepared by liquifying 33.8 g of the commercially available Muller Hinton agar medium in 1000 ml distilled water. The dissolved medium thus obtained was steamed at 15 lbs pressure at 121 °C for 15 min. Then the steamed medium was blended well and drained onto the 100 mm Petri plates (20–30 ml/plate) while molten and these Petri plates consisting of 20 ml MHA medium were sowed with bacterial culture of *E. coli (ATCC 25922)*, *P. aeruginosa* (ATCC 27853), *K. pneumonia (ATCC 13883)*, *S. mutans* (MTCC 890) and *S. aureus* (ATCC 25923) (growth of culture adjusted according to McFarland Standard, 0.5%). Then wells of 10 mm were drilled and varied concentrations of the sample such as 0.25 mg/ml, 0.5 mg/ml and 1.0 mg/ml were added. DMSO (10%) was used as the solvent for sample preparation. Then the plates were set at 37 °C for 24 h. The antibacterial capacity was determined by estimating the diameter of the inhibition zone created

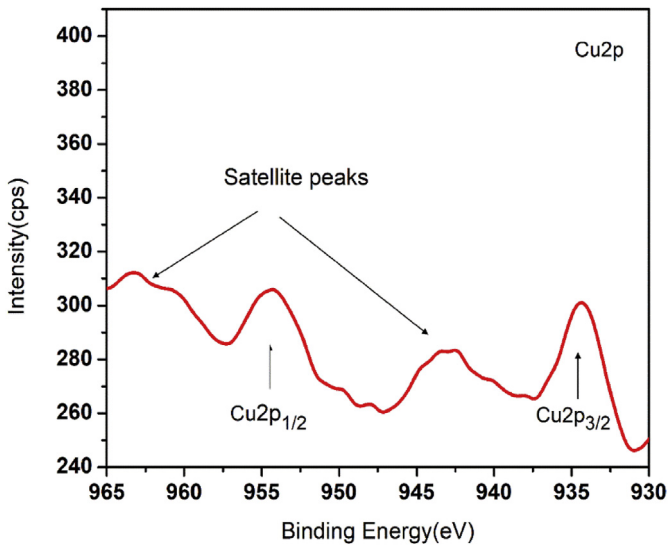

Figure 6. XPS signals of Cu2p.

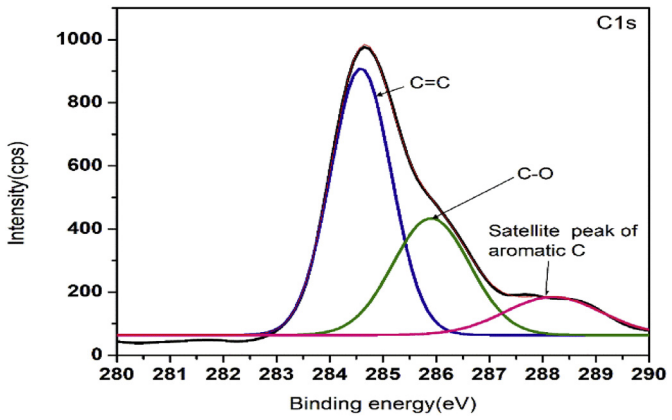

Figure 7. Deconvoluted XPS signal of C1s.

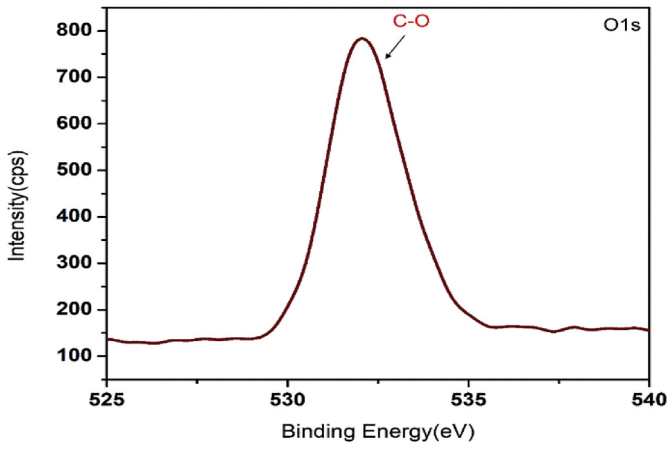

Figure 8. XPS signals of O1s.

around the well. In the antibacterial test, streptomycin was taken as a positive control.

Potato Dextrose Agar Medium (HiMedia) was used for fungal culture. The medium for the antifungal test was prepared by liquifying 39 g of commercially available Potato Dextrose Agar Medium in 1000 ml

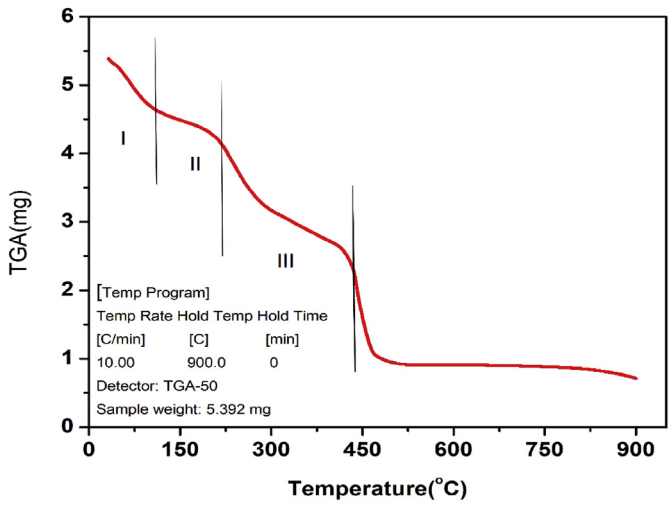

Figure 9. TGA curve exhibiting weight loss (mg)against temperature under an air atmosphere.

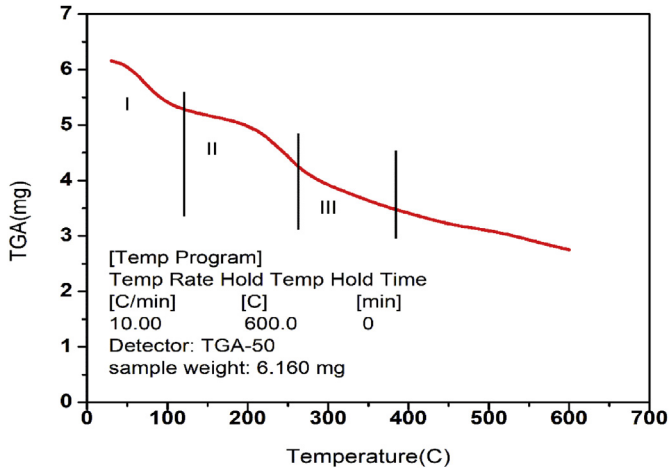

Figure 10. TGA curve exhibiting weight loss (mg)against temperature under nitrogen atmosphere.

distilled water. The liquified medium thus obtained was steamed at 15 lbs pressure at 121 °C for 15 min. The steamed medium was blended well and drained onto 100 mm Petri plates (20–30 ml/plate) while still molten. The fungi *A. niger* (ATCC 16404) and *C. albicans* (ATCC 10231) were grown overnight (growth of fungal culture adjusted according to McFarland Standard, 0.5%) and swabbed. Then the wells of 10 mm were drilled and samples of varying concentrations such as 0.250 mg/ml, 0.5 mg/ml and 1.0 mg/ml were added. The zone of inhibition in the anti-fungal test was measured after overnight incubation at room temperature and the activity was compared with that of a standard antimycotic (Clotrimazole). The detailed methods of antimicrobial tests are provided in the supplementary material.

The Minimum Inhibitory Concentration (MIC) was measured by using two-fold serial dilution method (Subcommittee on Antifungal Susceptibility Testing (AFST) of European Society of Clinical Microbiology and Infectious Diseases (ESCMID), European Committee for Antimicrobial Susceptibility Testing (EUCAST)," Method for determination of Minimum Inhibitory Concentration by broth dilution of fermented yeast", CMI, Vol.9,8,2003). The growth of inoculum (test organisms) was adjusted to 1% McFarland standard. The nutrient broth for this method was made by diluting 13 g of nutrient broth media in 1000 ml distilled water and autoclaved at 121 °C, 15 lbs for 15 min. The broth dilution assay was done in a 96 well microtiter plate. Each well in the plate was

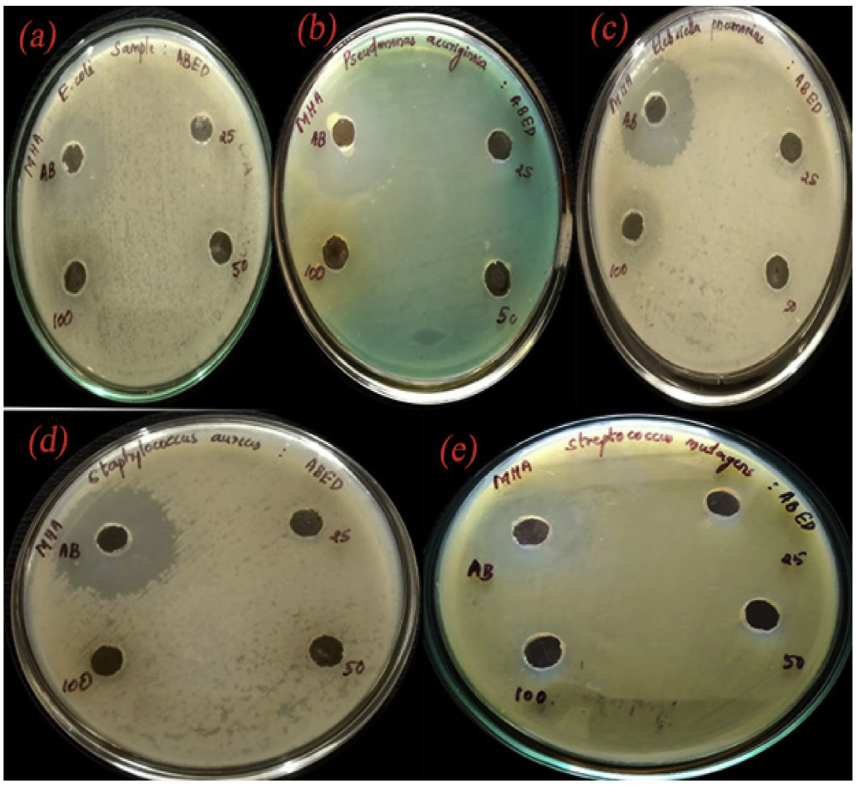

Figure 11. Photographs showing the zones of inhibition against the bacteria (a). *E. coli* (b). *P. aeruginosa* (c). *K. pneumoniae* (d). *S. aureus* and (e). *S. mutans.*

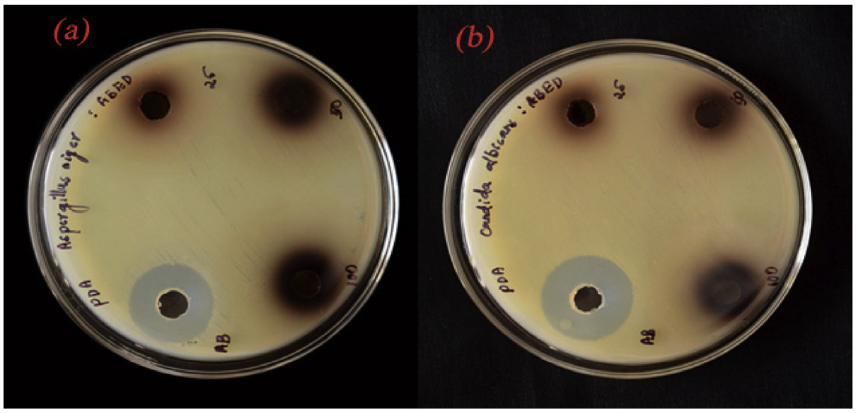

Figure 12. Photographs showing the zones of inhibition against the fungi (a). *A. niger* and (b). *C. albicans.*

added with 100 μl of the diluted conidial inoculum suspensions (two times) to make final volume in each well to 200 μl. The CuO/C nanocomposites were diluted in DMSO to a final concentration of 10 mg/ml and were added in various concentrations such as 0.0625mg, 0.125 mg, 0.250 mg, 0.5 mg, 1.0 mg to the wells and incubated overnight at room temperature. A control well was kept with the organism alone. Growth was observed by visual inspection and by estimating the optical density (OD) at 630 nm using ELISA plate reader. The OD was calculated quickly after the visual reading. The growth of inhibition for the wells taken for the antimicrobial test at each extract dilution was calculated by using the formula

$$\text{Percentage inhibition} = \frac{(\text{OD of control} - \text{OD of the test}) \times 100}{(\text{OD of control})} \quad (1)$$

The Minimum Fungicidal Concentration (MFC) and Minimum Bactericidal Concentration (MBC) tests were done using the CLSI protocol (CLSI Methods for determining bactericidal activity of antimicrobial agents. Approved guideline, NCCLS document M26-A, CLSI, 950, Wayne, USA). The materials required for the MBC test were the nutrient broth and Muller Hinton Agar (MHA) plates. The medium was made by liquifying 38 g of the MHA medium in 1000 ml distilled water. The liquified medium was steamed at 15 lbs at 121 °C for 15 min. After steaming, the media (20 ml) was allowed to cool to 60 °C and was poured to pre-sterilized Petri plates. Then the plates were permitted to solidify in a laminar airflow chamber. The nutrient broth of 23 g was dissolved in 1000 ml of distilled water and was steamed at 121 °C, 15 lbs for 15 min.

The minimum bactericidal activity was determined against *K. pneumonia*. The initial steps were done as in the MIC protocol. The sample concentration for the MBC test were 0.0625 mg, 0.125 mg, 0.250 mg, 0.5 mg, 1.0 mg, 1.5 mg and 2.0 mg. After 24 h of incubation, 20 μl from each well was swabbed onto MHA plates; the constituents of the well were not shaken before the removal of the definite volumes. The test

Table 1. Zones of inhibition (in diameter) shown by different bacteria.

Sample	Bacteria	Concentration (mg/ml)	Zone of inhibition Diameter (mm)
CuO/C nanocomposites	*E. coli*	Streptomycin (1mg)	23
		0.25	Nil
		0.5	Nil
		1.0	11
	Pseudomonas aeruginosa	Streptomycin (1mg)	28
		0.25	Nil
		0.5	Nil
		1.0	12
	Klebsiella pneumoniae	Streptomycin (1mg)	20
		0.25	Nil
		0.5	Nil
		1.0	14
	Staphylococcus aureus	Streptomycin (1mg)	30
		0.25	Nil
		0.5	Nil
		1.0	11
	Streptococcus mutans	Streptomycin (1mg)	22
		0.25	Nil
		0.5	Nil
		1.0	Nil

Table 2. Zones of inhibition (in diameter) shown by different fungi.

Sample	Organism	Concentration (mg/ml)	Zone of inhibition Diameter (mm)
CuO/C nanocomposites	*Aspergillus niger*	Clotrimazole (1mg)	22
		0.25	11
		0.5	12
		1.0	13
CuO/C nanocomposites	*Candida albicans*	Clotrimazole (1mg)	22
		0.25	11
		0.5	12
		1.0	14

plates were then incubated at 37 °C for 48 h. After incubation, the test plates were observed for the survival of colony-forming units (CFU). The minimum fungicidal activity was determined against the fungus *C. albicans*. The materials required for MFC were the nutrient broth and Potato Dextrose Agar (PDA) plates. The medium was made by diluting 39 g of the commercially available PDA in 1000 ml of distilled water. All the other parts of the MFC test was done as in the MBC test. The PDA test plates were incubated for 48 h and at room temperature.

3. Results and discussion

3.1. Characterization of nanocomposites

The formation of nanocomposites during the synthesis was indicated by a change in colour [22]. When the plant extract of hickory brown colour was added to the copper sulphate pentahydrate solution the light blue colour of copper sulphate solution changed to greenish-brown. Also, there was a pH change during the synthesis indicating the reduction reaction [42] and the formation of nanoparticles [43]. After the addition of plant extract (pH value 8.46), the pH of copper sulphate solution (pH value 5.39) was changed to 5. The alkaloids such as vasicine and vasicinone, tannins, saponins, proteins and phenols present in the leaf extract served as the reductant for the reduction of copper sulphate into copper and at the same time served as capping agents to avoid the further agglomeration of nanocomposites. The amino acids such as glycine, vitamin C and sugars existing in the leaf extract served as the source of carbon. However, the entire mechanism involved in the reduction process in the green synthesis of nanostructures using plants is still unknown.

3.1.1. UV-visible spectra analysis

The synthesized material was dispersed in distilled water and was used for the UV-Visible spectrum analysis. The spectrum recorded for the

Table 3. Percentage of inhibition against the bacteria *K. pneumonia* shown by the CuO/C nanocomposites in different concentrations.

Organism: *K. pneumonia*		
Group	Absorbance	Percentage of Inhibition
Control	0.2296	0.00
CuO/C nanocomposites Concentrations (mg/ml)		
0.625	0.2175	7.45
0.125	0.1851	19.38
0.250	0.1751	23.74
0.5	0.1233	46.30
1.0	0.1033	55.14

Table 4. Percentage of inhibition against the fungus *C. albicans* shown by the CuO/C nanocomposites in different concentrations.

Organism: *C. albicans*		
Group	Absorbance	Percentage of Inhibition
Control	0.2217	0.00
CuO/C nanocomposites Concentrations (mg/ml)		
0.625	0.2123	4.24
0.125	0.2030	8.43
0.250	0.1670	24.67
0.5	0.1349	39.15
1.0	0.1069	51.78

prepared nanocomposites is shown in the Figure 1. The surface plasmon vibration of the composites produced an absorption band centred at 282 nm which accords to the π - π* transition of aromatic sp^2 carbon domains [44]. The weak absorption band was assigned to the existence of reduced graphene oxide-like nanosheets demonstrating an effective exfoliation [45, 46]. The CuO nanoparticles also show the absorption band in the same region [47]. But, the quantity of CuO is very low and hence in the nanocomposite formation of CuO with Carbon a weak absorption band is formed. Also, there is no obvious band edge absorption found up to 700 nm. The figure represents the transient nature of absorption spectra in the visible range from 450 to 700nm which suggests the composites to find application in fluorescent materials [48, 49].

3.1.2. X-ray diffraction analysis

The XRD spectrum of synthesized nanocomposites is shown in Figure 2. The broad peaks centred at 29^o and 41^o are attributed to the graphene-like carbon present in the nanocomposites. The exfoliated carbon nanoflakes are formed during the synthesis of CuO/C nanocomposites and so the peaks of graphene-like carbon are weaker, suggesting the disordered stacking and agglomeration of carbon sheets in the nanocomposites [50]. Reduction in intensity of the peaks indicates that the volume of the sample that can diffract is lower for the composites which implies a better exfoliation of graphene-like carbon sheets in the CuO/C nanocomposites [51]. The characteristic peaks of CuO are not apparent in the XRD, suggesting the presence of small CuO nanoparticles with low crystallization, because of the presence of functional groups. The functional groups such as C=O present in the nanocomposites inhibit diffusion, crystallization and growing of CuO grains [52, 53, 54].

3.1.3. FTIR analysis

The comparison of the FTIR spectrum (Figure 3) of leaf powder and CuO/C nanocomposites gives an idea about the bonds in biomolecules which are capable of the reduction and the capping of nanocomposites. The peaks common to the spectra correspond to the bonds of biomolecules which are responsible for the stabilization of nanocomposites and sources of carbon. Some of the peaks are absent in the FTIR spectrum of CuO/C nanocomposites. This is as the consequence of either the breakage of bonds responsible for the reduction reaction or the absence of phytochemicals that are insoluble in water. In the FTIR spectrum of leaf powder the peaks at 635cm^{-1} and 984 cm^{-1} due to the alkyne C–H, 1074 cm^{-1} and 1192 cm^{-1} due to the C–C, 1462 cm^{-1} due to the C–H, 1632 cm^{-1} due to C=C stretch and 2895 cm^{-1} due to the C–H stretch represent the bonds corresponding to the phytochemicals such as alkaloids, proteins, sugars etc. present in the leaf. The peak at 2525 cm-1 indicates the thiol groups and 2062 cm-1 indicates the metal carbonyl groups in the leaves. In the FTIR spectrum of nanocomposites, the peaks at 1620 cm^{-1} due to the alkene C=C; 1447 cm^{-1} due to the aromatic C=C; 1115 cm^{-1} due to the C–O are originated from the biomolecules of the leaf extract. The new bond formation at 619 cm^{-1} is owing to the Cu–O bond formation [55, 56].

3.1.4. SEM-EDS analysis

The surface morphology and porosity of CuO/C nanocomposites were studied using SEM. The SEM images are shown in Figure 4. The software image J. was used to measure the images. The observable parts of the composite layers were considered for the measurement and the average values were calculated. The composite flakes have an average thickness7-11nm and the average interlayer distance between the flakes is 13–22 nm. Also, there is enough space between each stack, indicating the highly porous character of CuO/C nanocomposites.

The EDS data recorded from the CuO/C nanocomposites is as shown in Figure 5. The EDS profile shows the signals of copper along with oxygen and carbon. This supports the possibility of a composite development of copper oxide with carbon. The presence of carbon and oxygen is originated from the biomolecules present in the aqueous leaf extract. The major element present in the nanocomposites is carbon which is much greater than the percentage of oxygen. The percentage of copper is small compared to carbon and oxygen. The amount of sulphur is too small compared to other elements.

3.1.5. XPS analysis

XPS is a strong technique for analysing the chemical composition of materials. The oxidation state of copper oxide and nature of hybridisation of carbon were studied using the XPS. In the XPS profile, we got the characteristic copper peaks along with carbon and oxygen. The result is similar to that we obtained from the EDS analysis. The characteristic peak of Cu2p is shown in Figure 6. The peaks at 933.7 eV and 953.4 eV are assigned to the $Cu2p_{3/2}$ and $Cu2p_{1/2}$ binding energy values for Cu (II) [57, 58]. There is no much intensity difference between the peaks of $Cu2p_{3/2}$ and $Cu2p_{1/2}$. This is due to the oxide layers present in the nanocomposites. The emergence of the two strong satellite peaks near to $Cu2p_{3/2}$ and $Cu2p_{1/2}$ and the binding energy difference of 19.7 eV between $Cu2p_{3/2}$ and $Cu2p_{1/2}$further confirms the presence of Cu (II) ions [59]. The Cu (II) ion has an observable collection of satellite features at

Table 5. Table exhibiting the MBC determination of CuO/C nanocomposites against *K. pneumonia*.

Organism: *K. pneumonia*	
Group	CFU/ml
Control	4144
CuO/C nanocomposites (mg/ml)	
0.0625	116
0.125	92
0.25	56
0.5	40
1.0	12
1.5	1
2.0	NIL

Table 6. Table exhibiting the MFC determination of CuO/C nanocomposites against *C. albicans*.

Organism: *C.albicans*	
Group	CFU/ml
Control	424
CuO/C nanocomposites (mg/ml)	
0.0625	24
0.125	20
0.25	12
0.5	11
1.0	3
1.5	NIL
2.0	NIL

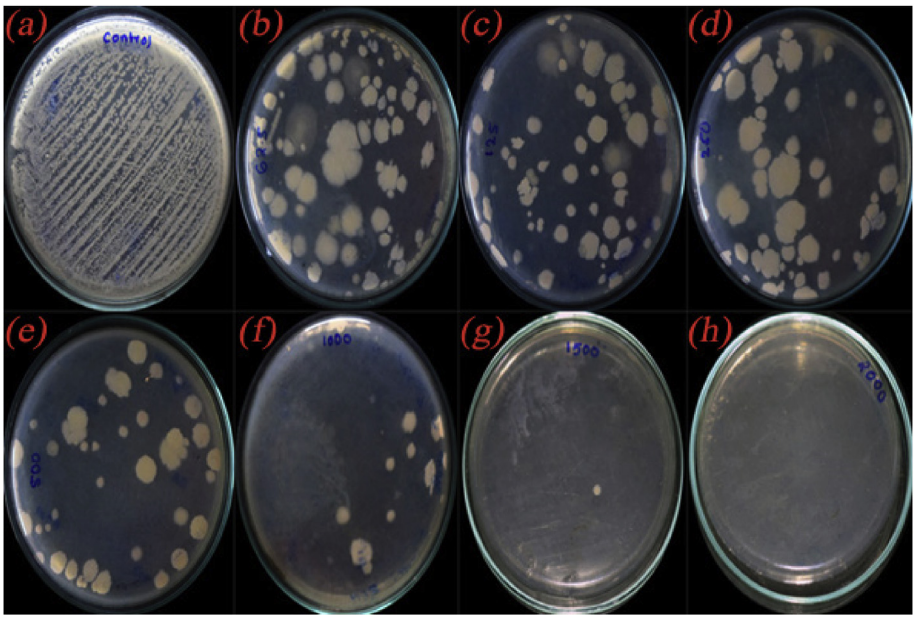

Figure 13. Photographs showing the antibacterial activity of (a) control and CuO/C nanocomposites in different concentrations (b) 0.0625 mg/ml (c) 0.125 mg/ml(d) 0.250 mg/ml (e) 0.5 mg/ml (f) 1.0 mg/ml (g)1.5 mg/ml (h) 2.0 mg/ml against the bacteria *K. pneumonia*.

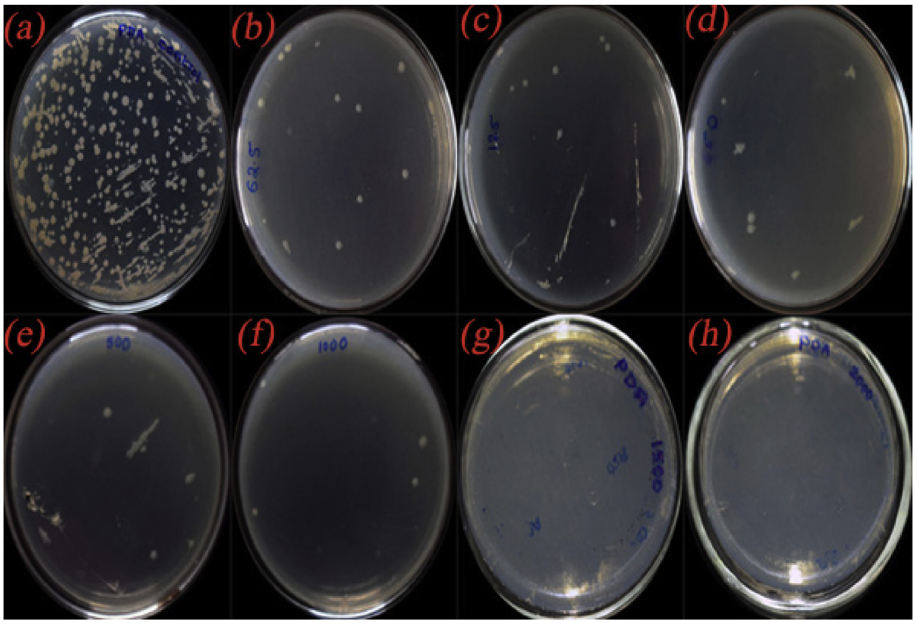

Figure 14. Photographs showing the antifungal activity of (a) control and CuO/C nanocomposites in different concentrations (b) 0.0625 mg/ml (c) 0.125 mg/ml(d) 0.250 mg/ml (e) 0.5 mg/ml (f) 1.0 mg/ml (g)1.5 mg/ml (h) 2.0 mg/ml against the fungus *C. albicans*.

943 eV, but for Cu(I)ions the satellite is weak. Also, the strong satellite peak near to $Cu2p_{1/2}$ is absent in the XPS spectra of Cu(I) [60]. The deconvolution of the C1s signal at 280–290 eV is shown in Figure 7. The peak at 284.4 eV originates from the C=C present in the nanocomposites. This implies that the majority of the carbon is present in the sp^2hybridization state. The peak at 286.1 eV is assigned to the C–O in the CuO/C nanocomposites and the weak peak centred at 288.6 eV is contributed to the shake-up feature of carbon in the aromatic compounds which results from the $\pi \rightarrow \pi^*$ transition. π bond is a characteristic of sp^2 hybridized carbons. The peak associated with C=C is more predominant than the peak associated with C–O. Hence most of the C atoms present in the CuO/C nanocomposites are in sp^2 hybridized form [54]. The characteristic peak of O1s signal is shown in Figure 8. The main strong peak at 532 eV is assigned to C–O present in the nanocomposites. The fitting up of the weak peak centred at 528.6 eV due to Cu–O in O1s spectra is difficult due to the large width of the peak. This is because the amount of CuO is very small compared to carbon and oxygen [61, 62, 63].

3.1.6. Thermo gravimetric analysis

The thermogravimetric analysis of the CuO/C nanocomposites was done both in the air (Figure 9) and in the nitrogen atmosphere (Figure 10). The TGA of nanocomposites under air gave a three-step degradation curve. The first step is due to the escape of water content and the other volatile components present in the sample. Above 100° the decomposition is due to the pyrolysis of oxygen-holding functional groups present in the plant extract giving CO_2, CO or H_2O vapours. The

third step is due to the combustion of carbonaceous materials. The TGA curve of the nanocomposites under nitrogen atmosphere also gave a three-step degradation curve. The first step of the curve is due to the escape of volatile components. In a nitrogen atmosphere, no oxidation or reduction takes place. However, the volatile components, water molecules and the volatile functional groups are degraded at respective temperatures in comparison with the TGA curve of nanocomposites obtained under air atmosphere. Under a nitrogen atmosphere, the functionalised graphene nanocomposites have better stability compared to the amorphous carbon materials. The main weight loss of functionalised graphene nanocomposites occurs only at about 500 °C. This is due to the more stable oxygen-carrying functional groups present in the nanocomposites. Under a nitrogen atmosphere, the TGA curve obtained for the CuO/C nanocomposites similar to that of the functionalised graphene nanocomposites. The amorphous carbon contaminates have lower oxidation temperatures (200°C–300 °C). If the carbon present in the nanocomposites is in the form of graphite oxide it will decompose at about 250 °C. But the CuO/C nanocomposites have a higher decomposition temperature. This is similar to the decomposition behaviour of functionalised graphene nanocomposites. Due to this special feature, the CuO/C nanocomposites can be used for thermal management of various materials [64].

3.2. Antimicrobial activity

The antimicrobial activity of the CuO/C nanocomposites against the bacteria *E. coli, P. aeruginosa, K. pneumoniae, S. aureus* and *S. mutans* and the fungi *A. niger* and *C. albicans* was studied by determining the diameter of their zones of inhibition against the microbes. The CuO/C nanocomposites showed significant zones of inhibition. The photographs showing the zones of inhibition by the nanocomposites against bacteria are shown in Figure 11 and fungi are shown in Figure 12. The clear images of Zone of Inhibition shown against *E. coli* (Figure S1), *P. aeruginosa* (Figure S2), *K. pneumoniae* (Figure S3), *S. aureus* (Figure S4), *S. mutans* (Figure S5), *A. niger* (Figure S6) and *C. albicans* (Figure S7) are given in the supplementary material provided with this article. Also, the original individual reports of zone of inhibition shown by the composite against *E. coli* (Table S1), *P. aeruginosa* (Table S2), *K. pneumonia* (Table S3), *S. aureus* (Table S4), *S. mutans* (Table S5), *A. niger* (Table S6) and *C. albicans* (Table S7) are presented in the supplementary material. The summary of zones of inhibition in terms of the diameter shown by the nanocomposites against the bacteria under study is given in Table 1 and against the fungi is given in the Table 2. The code ABED represents CuO/C nanocomposites and AB represents the control. The CuO/C nanocomposites exhibit the highest antibacterial performance against the gram-negative bacteria *K. pneumoniae* compared to the other four bacteria. The zone of inhibition with a zone diameter 14 mm was obtained in *K. pneumoniae.* The composites show no zone of inhibition against the bacteria *S. mutans.* The diameter of the zone of inhibition against the bacteria *E. coli* and *S. aureus* is 11mm. The CuO/C nanocomposites show antibacterial activity against both gram classes of bacteria. The zone of inhibition with a zone diameter 12 mm was obtained in the gram-negative bacteria *P. aeruginosa*. The diameter of the zone of inhibition against the fungi *A. niger* is 13 mm and *C. albicans* is 14 mm. The growth of inhibition may be due to the interruptions of cell membranes by the nanocomposites which result in break-down of cell enzyme [30]. All these results indicate that *A. vasica* mediated CuO/C nanocomposites show a significant antimicrobial property.

For the quantitative measurement of antimicrobial activity of the CuO/C nanocomposites, the MIC and MBC or MFC were determined. Two organisms *K. pneumonia* and *C. albicans* in which the composites showed better inhibition zone compared to other organisms were taken for the study. The Percentage of inhibition by the composites against *K. pneumonia* in varied concentrations is shown in Table 3 and that against the fungus *C. albicans* is shown in Table 4. The MIC value for the composites against *K. pneumonia* is calculated to be 0.791 mg/ml and against *C. albicans* is calculated to be 0.873 mg/ml (calculated using ED50 PLUS VI.0 software). The MBC or MFC was the minimal drug concentration that exhibited either no growing or fewer than 3 colonies to obtain 99–99.5 % extinction activity. The MBC measurement results against *K. pneumonia* are summarized in Table 5 and MFC measurement results against *C. albicans* are shown in Table 6. The photographs showing the antibacterial performance against the bacteria *K. pneumonia* by the composites in varied concentration are depicted in Figure 13 and the antifungal activity against *C. albicans* in different concentration are shown in Figure 14. The clear images of the MBC test in control (Figure S8) and the composites in various concentrations 0.0625 mg/ml (Figure S9), 0.125 mg/ml (Figure S10), 0.250 mg/ml (Figure S11), 0.5 mg/ml (Figure S12), 1.0 mg/ml (Figure S13), 1.5 mg/ml (Figure S14) and 2.0 mg/ml (Figure S15) and that of the MFC test in control well (Figure S16) and the composites in different concentrations 0.0625 mg/ml (Figure S17), 0.125 mg/ml (Figure S18), 0.250 mg/ml (Figure S19), 0.5 mg/ml (Figure S20), 1.0 mg/ml (Figure S21), 1.5 mg/ml (Figure S22) and 2.0 mg/ml (Figure S23) are provided in the supplementary material. The MBC and MFC of the composites are measured to be 1.5 mg/ml.

4. Conclusion

The proposed strategy for the synthesis of CuO/C nanocomposites using *A. vasica* leaf extract includes a novel, simple and eco-friendly procedures. From the FTIR, XPS and EDS analysis it is confirmed that the prepared material is a composite of CuO and Carbon. From the measurement of SEM images using software image J, the dimensions of the composites are found to be in the nano range. So, the prepared material is a nanocomposite of copper oxide and carbon. The TGA confirms the very important feature of the nanocomposite that the core structure of nanocomposite is functionalised graphene-like carbon embedded with copper oxide particles which are surrounded by the volatile functional groups. The CuO/C nanocomposites show significant antimicrobial activities against the gram-negative bacteria *P. aeruginosa, E. coli* and *K. pneumoniae* and the gram-positive bacteriae *S. aureus*, and the fungi *A. niger* and *C. albicans.*

5. Future prospective

Eco-friendly supercapacitors with CuO/C nanocomposites as material and nano-cellulose papers as substrates can be fabricated and these supercapacitors can be substituted for the usual supercapacitors.

Declarations

Author contribution statement

Bhavyasree P G & Xavier T S: Conceived and designed the experiments; Performed the experiments; Analyzed and interpreted the data; Contributed reagents, materials, analysis tools or data; Wrote the paper.

Funding statement

This research did not receive any specific grant from funding agencies in the public, commercial, or not-for-profit sectors.

Competing interest statement

The authors declare no conflict of interest.

Additional information

Supplementary content related to this article has been published online at https://doi.org/10.1016/j.heliyon.2020.e03323.

Acknowledgements

The authors are grateful to Amrita Centre for Medical Science, Kochi; Govt. College for women, Trivandrum for their support and FIST program, DST, Govt. of Kerala, India for providing research facilities.

References

[1] Y.S. Kim, I.S. Hwang, S.J. Kim, C.Y. Lee, CuO nanowire gas sensors for air quality control in an automotive cabin, Sens. Actuators B 135 (2008) 298–303.
[2] A. Umar, M.M. Rahman, A. Al-Hajry, Y.B. Hahn, Enzymatic glucose biosensor based on flower-shaped copper oxide nanostructures composed of thin nanosheets, Electrochem. Commun. 11 (2009) 278–281.
[3] S. Yang, C. Wang, L. Chen, S. Chen, Facile dicyandiamide-mediated fabrication of well- defined CuO hollow microspheres and their catalytic application, Mater. Chem. Phys. 120 (2010) 296–301.
[4] T. Yu, F.C. Cheong, C.H. Sow, The manipulation and assembly of CuO nanorods with line optical tweezers, Nanotechnology 15 (2004) 1732–1736.
[5] P. Podhajecky, B. Klapste, P. Novak, J. Mrha, R. Moshtev, V. Manev, A. Nassalevska, The influence of preparation conditions on the electrochemical behaviour of CuO in a Li/CuO cell, J. Power Source 14 (1985) 269–275.
[6] T. Ishihara, M. Higuchi, T. Takagi, M. Ito, H. Nishiguchi, T. Takita, Preparation of CuO thin films on porous $BaTiO_3$ by self-assembled multilayer film formation and application as a CO_2 sensor, J. Mater. Chem. 8 (1998) 2037–2042.
[7] T. Ishihara, K. Kometani, M. Hasida, Y. Takita, Application of mixed oxide capacitor to the selective carbon dioxide sensor, J. Electrochem. Soc. 138 (1991) 173–176.
[8] J. Tamaki, K. Shimanoe, Y. Yamada, Y. Yamamoto, N. Miura, N. Yamazoe, Dilute hydrogen sulphide sensing properties of CuO-SnO_2 thin film prepared by a low-pressure evaporation method, Sens. Actuators B 49 (1998) 121–125.
[9] R.V. Kumar, R. Elgamiel, Y. Diamant, A. Gedanken, Sonochemical preparation and characterization of nanocrystalline copper oxide embedded in polyvinyl alcohol and its effect on crystal growth of copper oxide, J. Norwig. Langmuir 17 (2001) 1406–1410.
[10] G. Borkow, R.C. Zatcoff, J. Gavia, Reducing the risk of skin pathologies in diabetics by using copper impregnated socks, Med. Hypotheses 73 (2009) 1–4.
[11] S.Y. Chaudhari, Assessment of genotoxic potential of tamra bhasma(incinerated copper), Int. J. Green Pharm. 9 (3) (2015) 175–179.
[12] S. Liu, T.H. Zeng, M. Hofmann, E. Burcombe, J. Wei, R. Jiang, J. Kong, Y. Chen, Antibacterial activity of graphite, graphite oxide, graphene oxide and reduced graphene oxide: membrane and oxidative stress, ACS Nano 5 (9) (2011) 6971–6980.
[13] K. Krishnamoorthy, N. Umasuthan, R. Mohan, J. Lee, S.J. Kim, Investigation of the antibacterial activity of graphene oxide nanosheets, J. Sci. Adv. Mater. 4 (2012) 1–7.
[14] A. Sharma, M. Varshney, S.S. Nanda, H.J. shin, N. Kim, D.k. Yi, K.H. Chae, S.O. Won, Structural, electronic structure and antibacterial properties of graphene-oxide nano-sheets 698 (2018) 85–92.
[15] S. Szunerits, R. Boukherroub, Antibacterial activity of graphene-based materials, J. Mater. Chem. 4 (2016) 6892–6912.
[16] J. Chen, H. Peng, X. Wang, F. Shao, Z. Yuan, H. Han, Graphene oxide exhibits broad-spectrum antimicrobial activity against bacterial phytopathogens and fungal conidia by intertwining and membrane perturbation, Nanoscale 6 (3) (2014) 1879–1889.
[17] S.R.K. Kumar, G.P. Mamatha, H.B. Muralidhara, M.S. Anantha, S. Yallappa, B.S. Hungund, K.Y. Kumar, Highly efficient multipurpose graphene oxide embedded with copper oxide nanohybrid for electrochemical sensors and biomedical applications, J. Sci. Adv. Mater. Devices 2 (2017) 493–500.
[18] K.A. Whitehead, M. Vaidya, C.M. Liauw, D.A.C. Brownson, P. Ramalingam, J. Kamieniak, S.J.R. Neale, L.A. Tetlow, J.S.T.W. Nieuwenhuis, D. Brown, A.J. McBain, J. Kulandaivel, C.E. Banks, Antimicrobial activity of graphene oxide-metal hybrids, Int. Biodeterior. Biodegrad. 123 (2017) 182–190.
[19] Z. Yang, X. Hao, S. Chen, Z. Ma, W. Wang, C. Wang, L. Yue, H. Sun, Q. Shao, V. Murugadoss, Z. Guo, Long-term antibacterial stable reduced graphene oxide nanocomposites loaded with cuprous oxide nanoparticles, J. Colloid Interface Sci. 533 (2019) 13–23.
[20] J.Y. Song, B.S. Kim, Biological synthesis of platinum nanoparticles using *Diopyroskaki* leaf extract, Bioproc. Biosyst. Eng. 33 (2010) 159–164.
[21] M.C. Reddy, K.S.R. Murthy, A. Srilakshmi, K.R.S.S. Rao, Phytosynthesis of eco-friendly silver nanoparticles and biological applications-a novel concept in nanobiotechnology, Afr. J. Biotechnol. 14 (3) (2015) 222–247.
[22] H.J. Lee, J.Y. Song, E.Y. Leon, B.S. Kim, Biological synthesis of copper nanoparticles using *magnolia Kobus* leaf extract and their antibacterial activity, J. Chem. Technol. Biotechnol. 88 (2013) 1971–1977.
[23] P. Yugandhar, T. Vasavi, P.U.M. Devi, Bioinspired green synthesis of copper oxide nanoparticles from *Syzygium alternifolium* (Wt.) Walp: characterization and evaluation of its synergistic antimicrobial and anticancer activity, Appl. Nanosci. 7 (2017) 417.
[24] K. Vishveshvar, M.V.A. Krishnan, K. Haribabu, S.V. Prasad, Green synthesis of copper oxide nanoparticles using Ixiro coccinea plant leaves and its characterization, BioNanoScience 8 (2018) 554–558.
[25] B.K. Sharma, D.V. Shah, D.R. Roy, Green synthesis of CuO nanoparticles using Azadirachta indica and its antibacterial activity for medicinal applications, Mater. Res. Express 5 (2008).
[26] P. Narasaiah, B.K. Mandal, N.C. Sarada, Biosynthesis of copper oxide nanoparticles from *Drypetes sepiaria* leaf extract and their catalytic activity to dye degradation, Mater. Sci. Eng. 263 (2017).
[27] F. Ijaz, S. Shahid, S.A. Khan, W. Ahmad, S. zaman, Green synthesis of copper oxide nanoparticles using abutilon indicum leaf extract: antimicrobial, antioxidant and photocatalytic dye degradation activities, Trop. J. Pharmaceut. Res. 16 (4) (2017) 743.
[28] J.M. Chung, A.A. Rahuman, S. Marimuthu, A.V. Kirthi, K. Anbarasan, P. Padmini, G. Rajakumar, Green synthesis of copper nanoparticles using Eclipta prostrata leaves extract and their antioxidant and cytotoxic activities, Exp. Therapeut. Med. 17 (2017) 18–24.
[29] Y. Abboud, T. Saffaj, A. Chagraoui, A.E. Bouari, K. Brouzi, O. Tanane, B. Ihssane, Biosynthesis, the characterization and antimicrobial activity of copper oxide nanoparticles (CONPs)produced using brown alga extract (*Bifurcaria bifurcata*), Appl. Nanosci. 4 (2014) 571–576.
[30] R. Sivaraj, P.K.S.M. Rahman, P. Rajiv, S. Narendhran, R. Venckatesh, Biosynthesis and characterization of *Acalypha indica* mediated copper oxide nanoparticles and their evaluation of its antimicrobial and anticancer activity, Spectrochim. Acta Mol. Biomol. Spectrosc. 129 (2014) 255–258.
[31] A. Mewada, S. Pandey, S. Shindey, N. Mishra, G. Oza, M. Thakur, M. Sharon, M. Sharon, Green synthesis of biocompatible carbon dots using an aqueous extract of *Trapa bispinosa* peel, Mater. Sci. Eng. 33 (2013) 2914–2917.
[32] J.X. Zheng, X. Liu, Y. Yang, X. Liu, B. Xu, Rapid and green synthesis of fluorescent carbon dots from starch for white light-emitting diodes, N. Carbon Mater. (2018) 33.
[33] W. Lu, X. Qin, S. Liu, G. Chang, Y. Zhang, Y. Luo, A.M. Asiri, A.O. Youbi, X. Sun, Economical, green synthesis of fluorescent carbon nanoparticles and their use as probes for sensitive and selective detection of mercury(II)ions, Anal. Chem. 84 (2012) 5351–5357.
[34] V. Sharma, P. Tiwari, S. M. Mobin, Sustainable carbon dots: recent advances in green carbon dots for sensing and bioimaging, J. Mater. Chem. B 5 (2017) 8904–8924.
[35] T.P. Singh, O.M. Singh, H.B. Singh, *Adhatoda vasica* Nees: phytochemical and pharmacological profile, Nat. Prod. J. 1 (2011) 29–39.
[36] S. Maurya, D. Singh, Quantitative analysis of total phenolic content in *Adhatoda vasica* Nees extract, Int. J. Pharm. Technol. 2 (4) (2010) 2403–2406.
[37] A. Karthikeyan, V. Shanthi, A. Nagasathaya, Preliminary phytochemical and antibacterial screening of crude extract of the leaf of Addhatoda vasica. L, Int. J. Green Pharm. (2009) 78–80.
[38] N. Chattopadhyay, G. Nosalova, S. Saha, S.S. Bandyopadhyay, D. Fleskova, B. Ray, Structural features and antitussive activity of water extracted polysaccharide from *Adhatoda vasica*, Carbohydr. Polym. 83 (2011) 1970–1974.
[39] D.K. Jha, L. Panda, P. Lavanya, S. Ramaiah, A. Anbarasu, Detection and Confirmation of alkaloids in leaves of adhatoda and bioinformatics approach to elicit its anti-tuberculosis activity, Appl. Biochem. Biotechnol. 168 (2012).
[40] P.R. Kanthale, V.H. Panchal, Pharmacognostic study of adhatoda vasica Nees, Biosci. Discov. 6 (1) (2014) 49–53.
[41] A.H. Amin, D.R. Mehta, A bronchodilator alkaloid (vasicinone) from *Adhatoda vasica* Nees, Nature 1317 (1959) 184.
[42] A. Mechler Sirajuddin, A.A.J. Torriero, A. Nafady, C.Y. Lee, A.M. Bond, A.P.O. Mullane, S.K. Bhargava, The formation of gold nanoparticles using hydroquinone as reducing agent through a localised pH change upon addition of NaOH to a solution of $HAuCl_4$, Colloids Surfaces A Physicochem. Eng. Aspects 370 (2010) 35–41.
[43] M. Singh, I. Sinha, R.K. Mandal, Role of pH in the green synthesis of silver nanoparticles, Mater. Lett. 63 (2009) 425–427.
[44] S. Gupta, T. Smith, A. Banaszak, J. Boeckl, Graphene quantum dots electrochemistry and sensitive electrocatalytic glucose sensor development, Nanomaterials 7 (10) (2017) 301.
[45] B.K. Ling, Carbon nanomaterials based on graphene nanosheets, in: Chapter 6, Taylor & Francies Group, New York, 2017, pp. 420–421.
[46] W. Ye, X. Li, H. Zhu, X. Wang, S. Wang, H. Wang, R. Sun, Green fabrication of cellulose/graphene composite in ionic liquid and its electrochemical and photothermal properties, Chem. Eng. J. 299 (2016) 45–55.
[47] W. Chen, J. Chen, Y. Feng, L. Hong, Q. Chen, L. Wu, X. Lin, X. Xia, Peroxidase-like activity of water soluble cupric oxide nanoparticles and its analytical application for detection of hydrogen peroxide and glucose, Analyst 137 (2012) 1706–1712.
[48] D. Li, M.B. Muller, S. Gilje, R.B. Kaner, G.G. Wallace, Processable aqueous dispersions of graphene nanosheets, Nat. Nanotechnol. 3 (2008) 101–105.
[49] J. Shang, L. Ma, J. Li, W. Ai, T. Yu, G.G. Gurzadyan, The origin of fluorescence from graphene oxide, Sci. Rep. 2 (2012) 792.
[50] Y. Zhao, X. Song, Q. Song, Z. Yin, A facile route to synthesis copper oxide/reduced graphene oxide nanocomposites and electrochemical detection of catechol organic pollutant, CrystEngComm 14 (2012) 6710–6719.
[51] C. Monteserin, M. Blanco, E. Aranzabe, A. Aranzabe, J.M. Laza, A.L. Varga, J.L. Vilas, Effects of graphene oxide and chemically reduced graphene oxide on the dynamic mechanical properties of epoxy amine composites 9 (9) (2017) 449.
[52] Y.J. Mai, X.L. Wang, J.Y. Xiang, Y.Q. Qiao, D. Zhang, C.D. Gu, J.P. Tu, CuO/graphene composite as anode materials for lithium-ion batteries, Electrochim. Acta 56 (2011) 2306–2311.
[53] R.M. Alwan, Q.A. Kadhim, K.M. Sahan, R.A. Ali, R.J. Mahdi, N.A. Kassim, A.N. Jassim, Synthesis of zinc oxide nanoparticles via sol-gel route and their characterization, Nanosci. Nanotechnol. 5 (1) (2015) 1–6.
[54] s. Drewniak, R. Muzyka, A. Stolarczyk, T. Pustelny, M.K. Moranska, M. setkiewicz, Studies of reduced graphene oxide and graphite oxide in the aspect of their possible application in gas sensors, Sensors 16 (2016) 103.

[55] N. Serin, T. Serin, S. Horzum, Y. Celik, Annealing effects on the properties of copper oxide thin films prepared by chemical deposition, Semiconductor, Sci. Technol. 20 (2005) 398–401.
[56] V.V.T. Padil, M. Cernik, Green synthesis of copper nanoparticles using gum karaya as a biotemplate and their antibacterial application, Int. J. Nanomed. 8 (2013) 889–898.
[57] T. Ghodselahi, M.A. Vesaghi, A. Shafiekhani, A. Baghizadeth, M. Lameii, XPS study of the Cu@Cu2O core-shell nanoparticles, Appl. Surf. Sci. 255 (2008) 2730–2734.
[58] X. Luo, C. Li, D. Yang, F. Liu, Y. Chen, Sonochemical synthesis of porous Cu2O-Cu hollow spheres and their photocatalysis, Mater. Chem. Phys. 151 (2015) 252–258.
[59] M.M. Rahman, M.M. Alam, M.M. Hussain, A.M. Asiri, M.E.M. Zaed, Hydrothermally prepared Ag_2O/CuO nanomaterial for an efficient chemical sensor development for environmental remediation, Environ. Nanotechnol. Monit. Manag. 10 (2018) 1–9.
[60] S. Sundar, G. Venkatachalam, S.J. Kwon, Biosynthesis of copper oxide (CuO) nanowires and their use for the electrochemical sensing of dopamine, Nanomaterials 8 (2018) 823.
[61] S.T. Jackson, R.G. Nuzzo, Determining hybridization differences for amorphous carbon from the XPS C1s envelope, Appl. Surf. Sci. 90 (1995) 195–203.
[62] W. Gao, L.B. Alemany, P.M. ajayan, New insights into the structure and reduction of graphite oxide, Nat. Chem. 1 (2009) 403–408.
[63] M.H. Ahmed, J.A. Byrne, J.M. Laughlin, W. Ahmed, Study of human serum albumin adsorption and conformational change on DLC and silicon doped DLC using XPS and FTIR spectroscopy, J. Biomater. Nanobiotechnol. 4 (2013) 194–203.
[64] M. Naebe, J. Wang, H. Khayyam, N. Hameed, L.H. Li, Y. Chen, B. Fox, Mechanical property and structure of covalent functionalised graphene/epoxy nanocomposites, Sci. Rep. (2014) 4375.